Atmos. Chem. Phys., 19, 12067–12082, 2019
https://doi.org/10.5194/acp-19-12067-2019

Atmospheric Chemistry and Physics
Open Access
EGU

Terrestrial ecosystem carbon flux estimated using GOSAT and OCO-2 XCO_2 retrievals

Hengmao Wang[1], Fei Jiang[1,2], Jun Wang[1], Weimin Ju[1], and Jing M. Chen[1,3]

[1]Jiangsu Provincial Key Laboratory of Geographic Information Science and Technology, International Institute for Earth System Science, Nanjing University, Nanjing, 210023, China
[2]Jiangsu Center for Collaborative Innovation in Geographical Information Resource Development and Application, Nanjing, 210023, China
[3]Department of Geography, University of Toronto, Toronto, Ontario M5S3G3, Canada

Correspondence: Fei Jiang (jiangf@nju.edu.cn)

Received: 7 November 2018 – Discussion started: 3 December 2018
Revised: 31 July 2019 – Accepted: 28 August 2019 – Published: 27 September 2019

Abstract. In this study, both the Greenhouse Gases Observing Satellite (GOSAT) and the Orbiting Carbon Observatory 2 (OCO-2) XCO_2 retrievals produced by the NASA Atmospheric CO_2 Observations from Space (ACOS) project (version b7.3) are assimilated within the GEOS-Chem 4D-Var assimilation framework to constrain the terrestrial ecosystem carbon flux during 1 October 2014 to 31 December 2015. One inversion for the comparison, using in situ CO_2 observations, and another inversion as a benchmark for the simulated atmospheric CO_2 distributions of the real inversions, using global atmospheric CO_2 trends and referred to as the poor-man inversion, are also conducted. The estimated global and regional carbon fluxes for 2015 are shown and discussed. CO_2 observations from surface flask sites and XCO_2 retrievals from Total Carbon Column Observing Network (TCCON) sites are used to evaluate the simulated concentrations with the posterior carbon fluxes. Globally, the terrestrial ecosystem carbon sink (excluding biomass burning emissions) estimated from GOSAT data is stronger than that inferred from OCO-2 data, weaker than the in situ inversion and matches the poor-man inversion the best. Regionally, in most regions, the land sinks inferred from GOSAT data are also stronger than those from OCO-2 data, and in North America, Asia and Europe, the carbon sinks inferred from GOSAT inversion are comparable to those from in situ inversion. For the latitudinal distribution of land sinks, the satellite-based inversions suggest a smaller boreal and tropical sink but larger temperate sinks in both the Northern and Southern Hemisphere than the in situ inversion. However, OCO-2 and GOSAT generally do not agree on which continent contains the smaller or larger sinks. Evaluations using flask and TCCON observations and the comparisons with in situ and poor-man inversions suggest that only GOSAT and the in situ inversions perform better than a poor-man solution. GOSAT data can effectively improve the carbon flux estimates in the Northern Hemisphere, while OCO-2 data, with the specific version used in this study, show only slight improvement. The differences of inferred land fluxes between GOSAT and OCO-2 inversions in different regions are mainly related to the spatial coverage, the data amount and the biases of these two satellite XCO_2 retrievals.

1 Introduction

Atmospheric inverse modeling is an effective method for quantifying surface carbon fluxes at global and regional scales using the gradient of CO_2 measurements. Inversion studies based on in situ CO_2 observations agree well on global carbon budget estimates but differ greatly on regional carbon flux estimates and the partitioning of land and ocean fluxes as well, mainly due to the sparseness of observations in the tropics, Southern Hemisphere oceans and the majority of continental interiors such as those in South America, Africa and boreal Asia (Peylin el al., 2013). Satellite observations offer an attractive means to constrain atmospheric inversions with their extensive spatial coverage over remote regions. Studies have shown that, theoretically, satellite observations,

though with lower precision than in situ measurements, can improve carbon flux estimates (Rayner and O'Brien, 2001; Park and Prather, 2001; Houweling et al., 2004; Baker et al., 2010; Chevallier et al., 2007; Miller et al., 2007; Kadygrov et al., 2009; Hungershoefer et al., 2010).

Satellite sensors designed specifically to retrieve atmospheric CO_2 concentrations have been in operation in recent years. The Greenhouse Gases Observing Satellite (GOSAT) (Kuze et al., 2009), being the first satellite mission dedicated to observing CO_2 from space, was launched in 2009. The National Aeronautics and Space Administration (NASA) launched the Orbiting Carbon Observatory 2 (OCO-2) satellite in 2014 (Crisp et al., 2017; Eldering et al., 2012, 2017a). China's first CO_2 monitoring satellite (TanSat) was launched in 2016 (Wang et al., 2017; Yang et al., 2018). These satellites measure near-infrared sunlight reflected from the surface in CO_2 spectral bands and the O_2 A band to retrieve column-averaged dry-air mole fractions of CO_2 (XCO_2), aiming to improving the estimation of the spatial and temporal distributions of carbon sinks and sources. A number of inversions have utilized GOSAT XCO_2 retrievals to infer surface carbon fluxes (Basu et al., 2013; Maksyutov et al., 2013; Saeki et al., 2013; Chevallier et al., 2014; Deng et al., 2014, 2016; Houweling et al., 2015). Although large uncertainty reductions were achieved for regions that are undersampled by in situ observations, these studies did not give robust regional carbon flux estimates. There are large spreads in regional flux estimates in some regions among these inversions. Furthermore, regional flux distributions inferred from GOSAT XCO_2 data are significantly different from those inferred from in situ observations. For instance, several studies using GOSAT retrievals reported a larger than expected carbon sink in Europe (Basu et al., 2013; Chevallier et al., 2014; Deng et al., 2014; Houweling et al., 2015). The validity of this large European carbon sink derived from GOSAT retrievals is in intense debate, and efforts to improve the accuracy of European carbon sink estimates are still ongoing (Reuter et al., 2014; Feng et al., 2016; Reuter et al., 2017).

Compared with GOSAT, OCO-2 has a higher sensitivity to column CO_2, much finer footprints and more extended spatial coverage, and it thus has the potential to better constrain surface carbon fluxes (Eldering et al., 2017b). Studies have used OCO-2 XCO_2 data to estimate carbon flux anomalies during recent El Niño events (Chatterjee et al., 2017; Patra et al., 2017; Heymann et al., 2017; Liu et al., 2017). Nassar et al. (2017) applied OCO-2 XCO_2 data to infer emissions from large power plants. Miller et al. (2018) evaluated the potential of OCO-2 XCO_2 data in constraining regional biospheric CO_2 fluxes and found that in the current state of development, OCO-2 observations can only provide a reliable constraint on the CO_2 budget at continental and hemispheric scales. At present, it is still not clear whether, with improved monitoring capabilities and better spatial coverage, current OCO-2 observations have greater potential than GOSAT observations for estimating CO_2 flux at a regional or finer scale, since the biases also affect the usefulness of satellite retrievals greatly. It is therefore important to investigate how current OCO-2 XCO_2 data differ from GOSAT XCO_2 data in constraining the carbon budget.

In this study, we evaluate the performance of GOSAT and OCO-2 XCO_2 data in constraining the terrestrial ecosystem carbon flux. GOSAT and OCO-2 XCO_2 retrievals produced by the NASA Atmospheric CO_2 Observations from Space (ACOS) team are applied to infer monthly terrestrial ecosystem carbon sinks and sources from October 2014 through December 2015 using a 4D-Var scheme based on the GEOS-Chem Adjoint model (Henze et al., 2007). For comparisons, one inversion based on in situ measurements is conducted, and another simple one, which uses the global CO_2 trend as a benchmark for the simulated atmospheric CO_2 distributions of the real inversion, is also implemented. For simplicity, the four inversions are referred to as the OCO-2 inversion, GOSAT inversion, in situ inversion and poor-man inversion. Inversion results are evaluated against surface flask CO_2 observations and Total Carbon Column Observing Network (TCCON) XCO_2 retrievals. This paper is organized as follows. Section 2 briefly introduces GOSAT and OCO-2 XCO_2 retrievals, surface observations, and the inversion methodology. Inversion settings are described in Sect. 3. Results and a discussion are presented in Sect. 4, and conclusions are given in Sect. 5.

2 Data and methods

2.1 GOSAT and OCO-2 XCO_2 retrievals

Developed jointly by the National Institute for Environmental Studies (NIES), the Japanese Space Agency (JAXA) and the Ministry of the Environment (MOE) of Japan, GOSAT was designed to retrieve total-column abundances of CO_2 and CH_4. The satellite flies at a 666 km altitude in a sun-synchronous orbit with 98° inclination that crosses the Equator at 12:49 local time. It covers the whole globe in 3 d and has a footprint of 10.5 km^2 at nadir. OCO-2 is NASA's first mission dedicated to retrieving atmospheric CO_2 concentration. It flies at 705 km of altitude in a sun-synchronous orbit with an overpass time at approximately 13:30 local time and a repeat cycle of 16 d. Its grating spectrometer measures reflected sunlight in three near-infrared regions (0.765, 1.61 and 2.06 µm) to retrieve XCO_2. OCO-2 has a footprint of 1.29×2.25 km^2 at nadir and acquires eight cross-track footprints, creating a swath width of 10.3 km.

Both GOSAT and OCO-2 XCO_2 products were created using the same retrieval algorithm, which is based on a Bayesian optimal estimation approach (Rodgers, 2000; O'Dell et al., 2012). The GOSAT and OCO-2 XCO_2 data used in this study are version 7.3 Level 2 Lite products at the pixel level. The XCO_2 data from Lite products are bias-corrected (Wunch et al., 2011). Before being used in our in-

version system, the data are processed in three steps. First, the retrievals for the glint soundings over oceans have relatively larger uncertainty, and thus the data over oceans are not used in our inversions (Wunch et al., 2017). Second, in order to achieve the most extensive spatial coverage with the assurance of using the best-quality data available, the XCO_2 data are filtered with two parameters, namely warn_levels and xco2_ quality_flag, which are provided along with the XCO_2 data. All data with the xco2_quality_flag not equaling 0 are removed, and the rest are divided into three groups according to the value of warn_levels: group 1, group 2 and group 3. In group 1, the warn_levels are less than 8; in group 2, the warn_levels are greater than 9 and less than 12, and in group 3, they are greater than 13. Group 1 has the best data quality, followed by group 2, and group 3 is the worst. Third, the pixel data are averaged within the grid cell of $2^\circ \times 2.5^\circ$, which is the resolution of the global atmospheric transport model used in this study. In each grid of $2^\circ \times 2.5^\circ$, only the groups of best data quality are selected and then averaged. The other variables, like column averaging kernel, retrieval error and so on, which are provided along with the XCO_2 product, are also handled with the same method. Figure 1a and b show the coverages and data amount of GOSAT and OCO-2 XCO_2 data during the study period after processing. The filtered GOSAT and OCO-2 retrievals are not evenly distributed spatially. Due to cloud contamination, there are few retrievals in a large portion of tropical land. In the northern high-latitude area, especially in boreal regions, due to the low soar zenith angle, available satellite retrievals are very sparse.

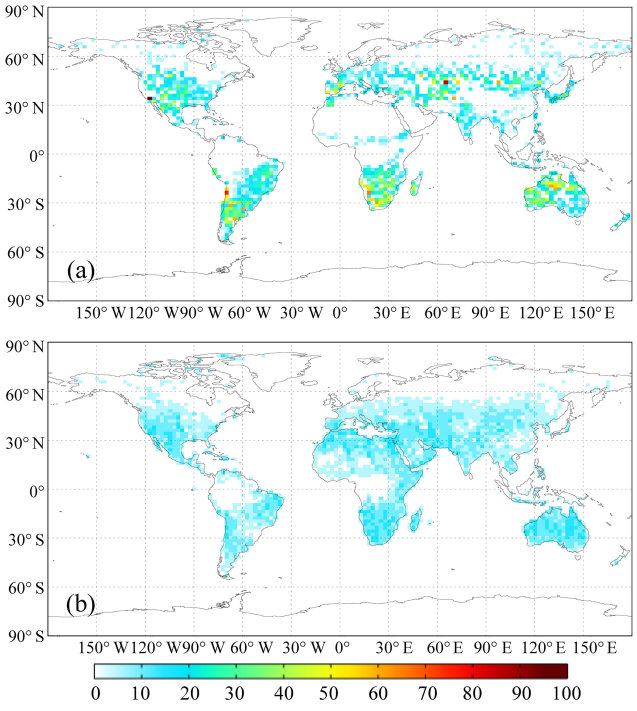

Figure 1. Data amount in each grid cell ($2^\circ \times 2.5^\circ$) of ACOS XCO_2 used in this study (**a**, GOSAT; **b**, OCO-2).

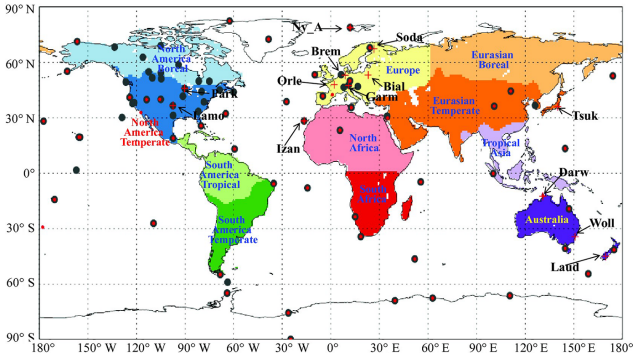

Figure 2. Distributions of the observation sites used in this study. Gray solid circles are surface sites used in the in situ inversion, red points and red cross marks are surface flask and TCCON sites used for evaluations, respectively, and the shaded area shows the 11 TRANSCOM regions.

2.2 Surface observations and TCCON XCO_2 retrievals

Surface CO_2 observations are from the obspack_co2_1_CARBONTRACKER_CT2016_2017-02-06 product (ObsPackCT2016) (CarbonTracker Team, 2017), which made up the observation data used in CarbonTracker 2016 (Peters et al., 2007, with updates documented at http://carbontracker.noaa.gov, last access: 10 August 2017). It is a subset of the Observation Package (ObsPack) data product (ObsPack, 2016) and contains a collection of discrete and quasi-continuous measurements at surface, tower and ship sites contributed by national universities and laboratories around the world. In this study, in situ measurements from 78 sites provided by this product are used for inversion. Among these 78 sites, there are 56 flask sites, of which 52 sites are selected to evaluate the posterior CO_2 concentrations (selection criteria given in Sect. 4.1.1).

TCCON is a network of ground-based Fourier transform spectrometers that measure direct near-infrared solar absorption spectra. Column-averaged abundances of atmospheric constituents including CO_2, CH_4, N_2O, HF, CO, H_2O and HDO are retrieved through these spectra. We use XCO_2 retrievals from 13 stations from the TCCON GGG2014 dataset (Blumenstock et al., 2017; Deutscher et al., 2017; Griffith et al., 2017a, b; Kivi et al., 2017; Morino et al., 2017; Notholt et al., 2017a, b; Sherlock et al., 2017; Sussmann and Rettinger, 2017; Warneke et al., 2017; Wennberg et al., 2017a, b). The 13 stations are Białystok (Bial), Bremen (Brem), Orleans (Orle), Garmisch (Garm), Darwin (Darw), Izana (Izan), Ny-Ålesund (Ny_A), Lamont (Lamo), Lauder (Laud), Park Falls (Park), Sodankylä (Soda), Tsukuba (Tsuk) and Wollongong (Woll). The locations of in situ sites and the 13 TCCON stations are shown in Fig. 2.

2.3 GEOS-Chem 4DVAR assimilation framework

2.3.1 GEOS-Chem model

The GEOS-Chem model (http://geos-chem.org, last access: 15 May 2017) is a global three-dimensional chemistry transport model (CTM), which is driven by assimilated meteorological data from the Goddard Earth Observing System (GEOS) of the NASA Global Modeling and Assimilation Office (GMAO) (Rienecker et al., 2008). The original CO_2 simulation in the GEOS-Chem model was developed by Suntharalingam et al. (2004) and accounts for CO_2 fluxes from fossil fuel combustion and cement production, biomass burning, terrestrial ecosystem exchange, ocean exchange, and biofuel burning. Nassar et al. (2010) updated the CO_2 simulation with improved inventories. In addition to the inventories in the earlier version, the new CO_2 fluxes includes CO_2 emissions from international shipping, aviation (3-D) and the chemical production of CO_2 from CO oxidation throughout the troposphere. In most other models, the oxidation of CO was treated as direct surface CO_2 emissions. The details of the CO_2 simulation and the CO_2 sink–source inventories can be found in Nassar et al. (2010). The version of the GEOS-Chem model used in this study is v8-02-01.

2.3.2 GEOS-Chem adjoint model

An adjoint model is used to calculate the gradient of a response function of one model scalar (or cost function) with respect to a set of model parameters. The adjoint of the GEOS-Chem model was first developed for the inverse modeling of aerosol (or their precursors) and gas emissions (Henze et al., 2007). It has been implemented to constrain sources of species such as CO, CH_4 and O_3 with satellite observations (Kopacz et al., 2009, 2010; Jiang et al., 2011; Wecht et al., 2012; Parrington et al., 2012). Several studies have successfully used this adjoint model to constraint carbon sources and sinks with surface flask measurements of CO_2 mixing ratio and space-based XCO_2 retrievals (Deng et al., 2014, 2016; Liu et al., 2014; Liu et al., 2017).

2.3.3 Inversion method

In the GEOS-Chem inverse modeling framework, the 4D-Var data assimilation technique is employed for combining observations and simulations to seek a best optimal estimation of the state of a system. The scaling factors are applied to the carbon flux components to be optimized monthly in each model grid point. This approach seeks the scaling factors of the carbon flux that minimize the cost function, J, given by

$$J(\mathrm{c}) = \frac{1}{2}\sum_{i=1}^{N}\left(\mathrm{XCO}_{2,i}^{\mathrm{m}} - \mathrm{XCO}_{2,i}^{\mathrm{obs}}\right) S_{\mathrm{obs},i}^{-1}\left(\mathrm{XCO}_{2,i}^{\mathrm{m}} - \mathrm{XCO}_{2,i}^{\mathrm{obs}}\right) + \left(\frac{1}{2}\left(c - c_{\mathrm{a}}\right) S_{\mathrm{c}}^{-1}\left(c - c_{\mathrm{a}}\right)\right), \quad (1)$$

where N is the total number of satellite XCO_2 observations; $\mathrm{XCO}_2^{\mathrm{m}}$ and $\mathrm{XCO}_2^{\mathrm{obs}}$ are the modeled and observed total-column averaged dry-air mole faction of CO_2, respectively; c_{a} is the prior scaling factor of the carbon flux, which is typically set as unity; S_{obs} is the model–data mismatch error covariance matrix; and S_{c} is the scaling factor error covariance matrix. The gradients of the cost function with respect to scaling factors calculated with the adjoint model are supplied to an optimization routine (the L-BFGS-B optimization routine; Byrd et al., 1994; Zhu et al., 1997), and the minimum of the cost function is sought iteratively.

For the modeled CO_2 column to be comparable with the satellite XCO_2 retrievals, the modeled CO_2 concentration profile should first be mapped into the satellite retrieval levels and then convoluted with retrieval averaging kernels. The modeled XCO_2 is computed by

$$\mathrm{XCO}_2^{\mathrm{m}} = \mathrm{XCO}_2^{\mathrm{a}} + \sum_j h_j a_j \left(A(x) - y_{a,j}\right), \quad (2)$$

where j denotes the retrieval level, x is the modeled CO_2 profile, $A(x)$ is a mapping matrix, $\mathrm{XCO}_2^{\mathrm{a}}$ is prior XCO_2, h_j is a pressure weighting function, a_j is the satellite column averaging kernel and y_{a} is the prior CO_2 profile for retrieval. These last four quantities are provided from ACOS version 7.3 Level 2 Lite products.

3 Inversion settings

In this study, the GEOS-Chem model was run at a horizontal resolution of $2^\circ \times 2.5^\circ$ for 47 vertical layers. Three inversions, using GOSAT data, OCO-2 data and in situ measurements, are conducted from 1 October 2014 to 31 December 2015. Poor-man inversion, based on the global atmospheric CO_2 trend and using the poor-man method (Chevallier et al., 2009, 2010), is also conducted. The posterior dry-air mole fraction of CO_2 on 1 October 2014 from the CT2016 product is taken as the initial concentration. The first 3 months are taken as the spin-up period. The prior carbon fluxes used in this study include fossil fuel CO_2 emissions, biomass burning CO_2 emissions, terrestrial ecosystem carbon exchange and CO_2 flux exchange over the sea surface. Fossil fuel emissions are obtained from CT2016, which is an average of the Carbon Dioxide Information Analysis Center (CDIAC) product (Andres et al., 2011) and the Open-source Data Inventory of Anthropogenic CO_2 (ODIAC) emission product (Oda and Maksyutov, 2011). The biomass burning CO_2 emissions are also taken from CT2016, which are the average of the Global Fire Emissions Database version 4.1 (GFEDv4) (van der Werf et al., 2010; Giglio et al., 2013) and the Global Fire Emission Database from NASA Carbon Monitoring System (GFED_CMS). The 3-hourly terrestrial ecosystem carbon exchanges are from the Carnegie–Ames–Stanford approach (CASA) model GFED4.1 simulation (Potter el al., 1993; van der Werf et al., 2010). CO_2 exchanges

over the ocean surface are from the posterior air–sea CO_2 flux of CT2016. It is noted that the fossil fuel emissions and the biomass burning emissions in our inversions are kept intact. Both terrestrial ecosystem CO_2 exchanges and ocean flux are optimized in our inversions.

An efficient computational procedure for constructing a non-diagonal scaling factor error covariance matrix that accounts for the spatial correlation of errors is implemented (Singh et al., 2011). The construction is based on the assumption of the exponential decay of error correlations. Other than forming the covariance matrix explicitly, multidimensional correlations are represented by tensor products of one-dimensional correlation matrices along longitude and latitudinal directions. For the two inversions, the scale lengths assigned along longitudinal and latitudinal directions are 500 and 400 km for terrestrial ecosystem exchange and 1000 and 800 km for ocean exchange, respectively. No correlations between different types of fluxes are assumed. The temporal correlations are also neglected. A global annual uncertainty of 100 % and 40 % is assigned for terrestrial ecosystem and ocean CO_2 exchanges, respectively (Deng and Chen, 2011). Accordingly, the uncertainty of the scaling factor for the prior land and ocean fluxes in each month at the grid cell level are assigned as 3 and 5, respectively.

3.1 Inversions using satellite XCO_2 retrievals

The observation error covariance matrix is constructed using the retrieval errors, which are provided along with the ACOS XCO_2 data. Observation errors are assumed to be uncorrelated at the model grid level. To account for the correlated observation errors, as shown in Sect. 2.1, the pixel-level retrieval errors are filtered and averaged to the model grid level and then inflated by a factor of 1.9 to ensure that the chi-square testing of the χ^2 value is close to 1 (Tarantola, 2004; Chevallier et al., 2007).

3.2 Inversion using in situ measurements

As described in Sect. 2.2, surface CO_2 observations from 78 sites, including flask samples and from a quasi-continuous analyzer, are adopted in this inversion. These data are selected from the data collection of ObsPackCT2016. The observation uncertainties of the 78 sites are also obtained from this product, which account for both measurement and representative errors (Peters et al., 2007, with updates documented at http://carbontracker.noaa.gov, last access: 10 August 2017). An examination for differences between observations and the forward model simulation was conducted (data not shown), and the results show that observation uncertainties from CT2016 represent the model–data mismatch errors of the GEOS-Chem model well. In addition, we neglect correlations between observations and assume a diagonal observation error covariance matrix.

3.3 Poor-man inversion

A baseline inversion, which was introduced by Chevallier et al. (2009, 2010) as a poor-man method, is implemented to evaluate satellite retrievals and in situ measurement-based inversions. Usually, the posteriori fluxes are evaluated by the improvement of the simulated CO_2 mixing ratios. Since the global CO_2 trend can be accurately estimated from marine sites, it is important to assess whether the inverted flux can capture more information than this trend. In this baseline inversion, the ocean flux is kept identical to the prior ones. The poor-man inverted land flux F_{pm} at location (x, y) and at time t is defined as

$$F_{\mathrm{pm}}(x, y, t) = F_{\mathrm{prior}}(x, y, t) + k \times \sigma(xyt), \tag{3}$$

where F_{prior} is the prior flux, σ is the uncertainty of the prior flux and k is a coefficient that can be solved directly from the formula (3) as

$$k = \left(\sum F_{\mathrm{pm}}(x,\, y,\, t) - \sum F_{\mathrm{prior}}(x,\, y,\, t)\right) / \sum \sigma(x,\, y,\, t), \tag{4}$$

where $\sum F_{\mathrm{pm}}(x,\, y,\, t)$ equals the global total land flux, which can be calculated from the observed annual global CO_2 growth rate, global annual fossil fuel and biomass burning emissions, and ocean flux. In this study, the observed annual global CO_2 growth rate is from the Global Monitoring Division (GMD) of the NOAA/Earth System Research Laboratory (ESRL) (Ed Dlugokencky and Pieter Tans; NOAA/ESRL, https://www.esrl.noaa.gov/gmd/ccgg/trends/, last access: 10 July 2018). The annual global CO_2 growth rate is 2.96 ppm in 2015, which is converted to 6.28 PgC yr^{-1} for the poor-man global total by multiplying by a factor of 2.123 PgC ppm^{-1}.

4 Results and discussion

4.1 Evaluation for the inversion results

4.1.1 Flask observations

As shown in Sect. 2.2, flask observations from 52 sites are used to evaluate the inversion results. Actually, there are many more flask observations in the dataset. When there is more than one flask dataset for one site, we give priority to that from NOAA/ESL or that with more consistent records. There are 56 sites with available flask observations for evaluation. In addition, during the evaluations, we find that the GEOS-Chem model is unable to capture the variations of CO_2 mixing ratios at the Hohenpeissenberg (HPB), Hegyhátsál (HUN), Southern Great Plains (SGP) and Tae-ahn Peninsula (TAP) sites, where the standard deviations between the observed and modeled mixing ratios are larger than 5 ppm. Therefore, we exclude these four sites and use the rest of the 52 flask sites (shown in Fig. 2) to evaluate the posterior mixing ratios. The GEOS-Chem model is driven with the prior

flux and the four posterior fluxes to obtain the prior and posterior CO_2 mixing ratios. The simulated CO_2 mixing ratios are sampled at each observation site and within half an hour of the observation time.

Table 1 shows a summary of comparisons of the simulated CO_2 mixing ratios against the flask measurements. The mean difference between the prior CO_2 mixing ratio and the flask measurements is 0.93 ppm, with a standard deviation of 2.3 ppm. All four inversions show improvement in posterior concentrations, with reductions of biases. Not surprisingly, in situ inversion, using surface observations that include all the flask measurements used for evaluation, shows the best improvement in the posterior CO_2 mixing ratio with the largest reduction of bias and standard deviation. GOSAT inversion achieves almost the same reductions of standard deviation as in situ inversion. OCO-2 inversion gives a larger bias and standard deviation than in situ and GOSAT inversions. Poor-man inversion effectively reduces the bias but with little improvement in the reduction of standard deviations.

Figure 3 shows the biases at each observation site at different latitudes. It could be found that the biases between the simulations and the observations in the Northern Hemisphere are significantly larger than those in the Southern Hemisphere since the carbon flux distribution of the Northern Hemisphere is more complex than that of the Southern Hemisphere. When the prior flux is used, almost all sites in the Northern Hemisphere have significant positive deviations, with an average of 1.7 ppm, while in the Southern Hemisphere, the deviations are very small, with an average bias of only −0.08 ppm; when using the posteriori flux from OCO-2 inversion, the deviations at most Northern Hemisphere sites are slightly reduced, with an average deviation of 0.85 ppm, while in the Southern Hemisphere, at most sites, the biases increase by variable amounts, with a mean of −0.13 ppm. When using the posterior flux from the GOSAT inversion, the deviations are significantly reduced to 0.04 ppm in the Northern Hemisphere but further increased to −0.55 ppm in the Southern Hemisphere. In situ inversion shows similar improvement in the Northern Hemisphere as GOSAT inversion, but also with little improvement in the Southern Hemisphere. Though poor-man inversion effectively reduces the global bias, it shows the largest negative biases in the Southern Hemisphere and moderate positive biases (close to OCO-2 inversions) in the Northern Hemisphere, indicating that improvements with poor-man inversion for posterior concentrations are very limited. This suggests that GOSAT and in situ inversions can effectively improve carbon flux estimates in the Northern Hemisphere but overestimate the land sinks in the Southern Hemisphere.

4.1.2 TCCON observations

We also use data from 13 TCCON sites (Fig. 2) to evaluate our inversion results. The simulated CO_2 concentrations at 47 vertical levels are mapped onto 71 TCCON levels. Following the approach of Wunch et al. (2011), using prior profiles and the averaging kernel from the TCCON dataset, we calculated the modeled XCO_2 values at 13 TCCON sites. It should be noted that comparisons of posterior XCO_2 from GOSAT and OCO-2 inversions with TCCON data are not fully independent since the TCCON data were used in the bias-correction scheme of both the GOSAT and OCO-2 products (Wunch et al., 2011). Table 1 also shows the comparison of modeled XCO_2 with TCCON observations. The mean difference between prior XCO_2 and TCCON retrievals is 1.16 ppm, with a standard deviation of 1.3 ppm. GOSAT inversion performs the best with the largest reductions of bias and standard deviation. Though OCO-2 inversion shows improvement in the reduction of standard deviation, it gives a relatively large bias for posterior XCO_2. In situ inversion has the same reduction of standard deviation as GOSAT inversion. Poor-man inversion reduces the bias to 0.49 ppm and gives slight improvement in reducing the standard deviation of posterior XCO_2.

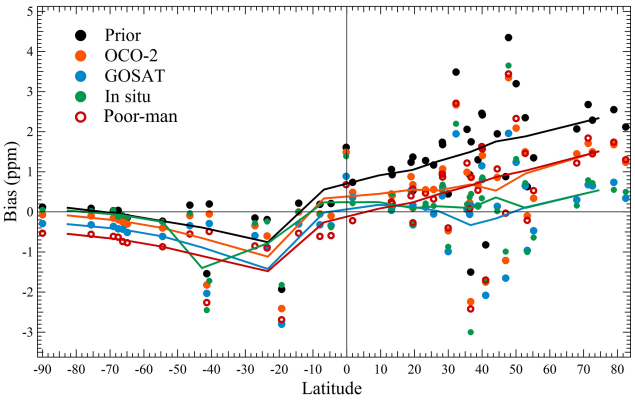

Figure 3. Biases of the simulated CO_2 mixing ratios against the flask measurements at different latitudes (positive–negative biases represent a modeled concentration greater–less than the observed, and the different colored lines represent the smoothing of the corresponding marks).

Figure 4 shows the bias at each TCCON site. Obviously, the biases at all TCCON sites are positive when using the prior fluxes, ranging between 0.3 and 2.6 ppm. The biases at the sites in the northern temperate and boreal areas are all above 1.5 ppm except for the Lamo site. GOSAT and in situ inversions significantly reduce the biases at most sites. However, in the Northern Hemisphere, the biases at those sites remain relatively large. Since GOSAT and in situ inversions show evident improvement at flask sites in the Northern Hemisphere, the remaining large biases at TCCON sites may also be related to the biases of TCCON retrievals (Wunch et al., 2010; Messerschmidt et al., 2011). OCO-2 and poor-man inversions show slight improvement in the reduction of biases at most sites, and rather large biases still remain.

Overall, it could also be found from Table 1 that only in situ inversion beats the poor-man inversion on all four statis-

Table 1. Statistics of the model–data mismatch errors at the 52 surface flask sites and the 13 TCCON sites (ppm).

	Flask		TCCON	
	Bias	SD	Bias	SD
Prior	0.93	2.30	1.16	1.30
OCO-2	0.33	2.15	0.80	1.08
GOSAT	−0.19	2.05	0.22	1.04
In situ	−0.03	2.04	0.38	1.04
Poor-man	0.14	2.28	0.49	1.25

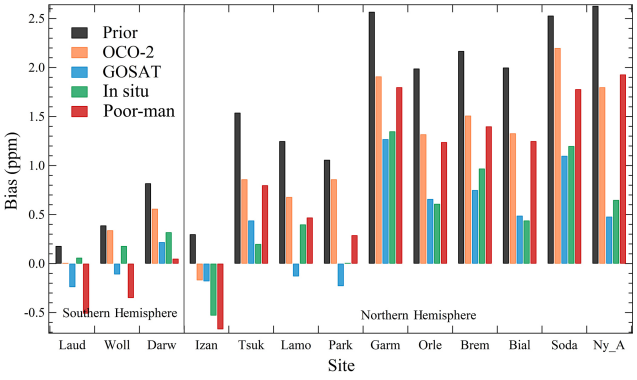

Figure 4. The biases between the modeled and observed XCO_2 at the 13 TCCON sites.

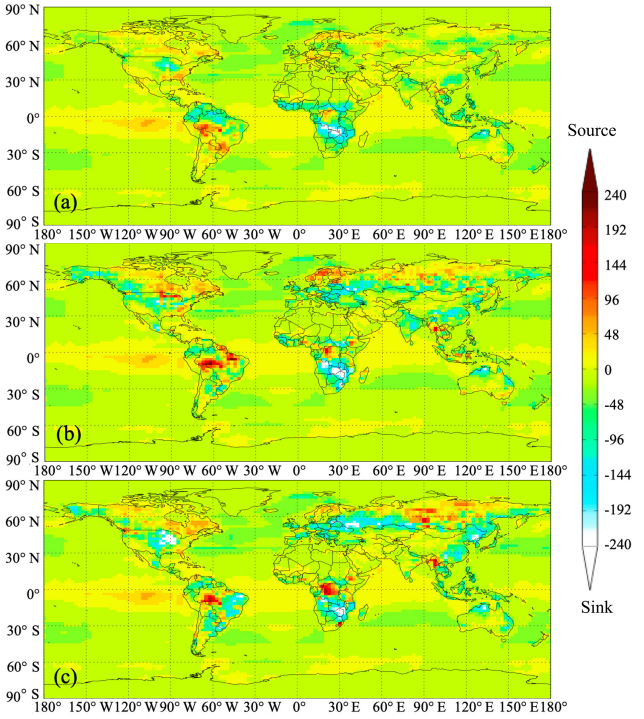

Figure 5. Distributions of annual land and ocean carbon fluxes; **(a)** prior flux and posterior fluxes based on **(b)** OCO-2 and **(c)** GOSAT data (gC m^{-2} yr^{-1}).

tics, followed by GOSAT inversion, which beats the poor-man on three statistics, indicating that in situ measurements have the best performance among all inversions and GOSAT retrievals have a similar performance as in situ data.

4.2 Global carbon budget

Table 2 presents the global carbon budgets in 2015 from the four inversions. The global land sinks inferred by GOSAT and OCO-2 XCO_2 retrievals are −3.48 and −2.94 PgC yr^{-1}, respectively, which are both larger than the prior value and lower than the estimate from the in situ inversion. The differences of ocean fluxes among the a priori and two inversions are small since we do not assimilate XCO_2 data over ocean. The global net flux from the poor-man inversion is inferred from the global annual CO_2 growth rate, which relatively accurately represents the net carbon flux added into atmosphere. It could be found that the global net flux from GOSAT inversion is the closest to the poor-man inversion estimate, while that from the OCO-2 inversion is higher and the in situ inversion estimate is lower than the poor-man estimate, indicating that GOSAT inversion has the best estimates for land and ocean carbon uptakes, while those from the in situ inversion are overestimated and those from the OCO-2 inversion might be underestimated.

4.3 Regional carbon flux

Figure 5 shows the distributions of annual land and ocean carbon fluxes (excluding fossil fuel and biomass burning carbon emissions, same thereafter) of the prior and estimates using GOSAT and OCO-2 data. It could be found that compared with the prior fluxes, the carbon sinks in Central America, southern and northeastern China, eastern and central Europe, southern Russia, and eastern Brazil are obviously increased in the GOSAT inversion. Except for eastern Brazil, the land sinks in those areas in the OCO-2 inversion are also increased but much weaker than those in the GOSAT inversion; in eastern Brazil, it turns into a significant carbon source. In contrast, in eastern and central Canada, northern Russia, northern Europe, the western Indo-China Peninsula, the northern Democratic Republic of the Congo, and western Brazil, carbon sources are significantly increased in both GOSAT and OCO-2 inversions. In eastern and central Canada, northern Europe, and western Brazil, there are much stronger carbon sources in the OCO-2 inversion.

To better investigate the differences between GOSAT and OCO-2 inversions as well as their differences from the other two inversions, we aggregate the prior and inferred land fluxes into 11 TRANSCOM land regions (Gurney et al., 2002) as shown in Fig. 2. Figure 6 shows aggregated annual land surface fluxes from the prior and inversions for the 11 land regions. Clearly, in most regions, the land sinks inverted

Table 2. Global carbon budgets estimated by the OCO-2 and GOSAT inversions in this study and those from the prior fluxes as well as in situ and poor-man inversions ($PgC\,yr^{-1}$).

	Prior	OCO-2	GOSAT	In situ	Poor-man
Fossil fuel and industry	9.84	9.84	9.84	9.84	9.84
Biomass burning emissions	2.20	2.20	2.20	2.20	2.20
Land sink	−2.50	−2.94	−3.48	−3.63	−3.35
Ocean sink	−2.41	−2.44	−2.45	−2.41	−2.41
Global net flux	7.13	6.66	6.11	6.00	6.28

based on GOSAT data are stronger than those inferred from OCO-2 data, especially in temperate and tropical lands. For example, in South American temperate, the estimated land sink based on GOSAT data is about 4 times as large as the OCO-2 inversions; in North American temperate and tropical Asia, the carbon sinks of the GOSAT experiment are about twice those of the OCO-2 inversions, and in South American tropical, the OCO-2 inversion result is a carbon source of $0.19\,PgC\,yr^{-1}$, while GOSAT inversion gives a weak sink of $-0.05\,PgC\,yr^{-1}$. The total sinks of the temperate–tropical lands optimized using GOSAT and OCO-2 XCO_2 retrievals are $-2.95/-0.36$ and $-2.59/-0.20\,PgC\,yr^{-1}$, respectively (Table 3). In northern boreal land, the total carbon sinks inverted with GOSAT and OCO-2 data are comparable. However, the two sets of XCO_2 data have opposite performances in two northern boreal regions. In Eurasian boreal, the inverted land sink with GOSAT is stronger than that with OCO-2, while in North American boreal, it is the opposite.

For different continents (Table 3), for example Asia and Australia, the carbon sinks inverted from GOSAT and OCO-2 data are comparable. In North America, South America and Europe, the land sinks in the GOSAT inversion are much stronger than those in the OCO-2 inversion. Especially in South America, the GOSAT inversion result is a strong carbon sink ($-0.51\,PgC\,yr^{-1}$), while in the OCO-2 inversion, it is a weak carbon source ($0.06\,PgC\,yr^{-1}$). Conversely, in Africa, the land sink estimated with GOSAT data is much weaker than that from OCO-2 data, the former ($-0.59\,PgC\,yr^{-1}$) being only about half of the latter ($-1.13\,PgC\,yr^{-1}$).

Compared with the in situ inversion, in boreal regions, the land sinks estimated from GOSAT and OCO-2 inversions are much weaker than those from in situ inversion, especially in the Eurasian boreal region; the land sink estimated by in situ inversion is more than 2 times larger than the estimates of GOSAT and OCO-2 inversions. In tropical land, the total land sinks inferred from both GOSAT and OCO-2 inversions are weaker than those from the in situ inversion, but in different regions, the situations are different. In the temperate lands, except for Europe and South Africa (a defined TRANSCOM region, as shown in Fig. 2), the land sinks from GOSAT and OCO-2 inversions are much stronger than those from the in situ inversion. For example, in South American

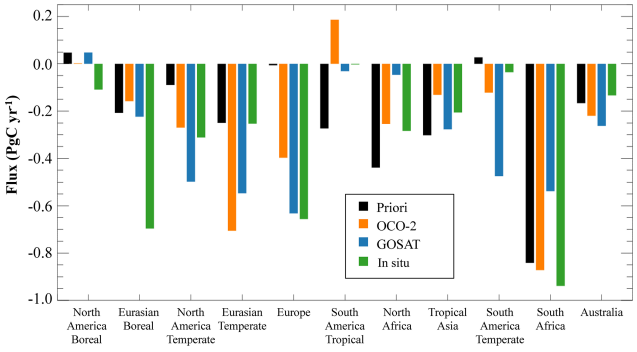

Figure 6. Aggregated annual land fluxes of the 11 TRANSCOM land regions.

Table 3. The prior and posterior fluxes on six continents and in boreal, temperate and tropical lands ($PgC\,yr^{-1}$).

Regions	Prior	OCO-2	GOSAT	In situ
North America	−0.04	−0.27	−0.45	−0.42
South America	−0.25	0.06	−0.51	−0.04
Europe	−0.01	−0.40	−0.63	−0.66
Asia	−0.76	−0.99	−1.05	−1.16
Africa	−1.28	−1.13	−0.58	−1.22
Australia	−0.17	−0.22	−0.26	−0.13
Northern boreal land	−0.16	−0.16	−0.18	−0.81
Northern temperate land	−0.35	−1.37	−1.68	−1.22
Tropical land	−1.01	−0.20	−0.36	−0.49
Southern temperate land	−0.98	−1.21	−1.28	−1.11

temperate, GOSAT inversion shows a strong carbon sink, while in situ inversion shows a weak source. For different continents, for example North America, Asia and Europe, the carbon sinks inferred from GOSAT inversion are comparable to those from in situ inversion, while in South America and Africa, the carbon sinks inferred from OCO-2 inversion are much closer to the in situ inversion.

Compared with the prior fluxes, the inferred land fluxes in northern temperate regions have the largest changes, followed by those in tropical regions and southern temperate lands, while in boreal regions, the changes are the smallest. As shown in Table 4, for different TRANSCOM regions and different XCO_2 used, the changes in carbon fluxes have large differences. Since the same setup is used in these two

inversions and the same algorithm is adopted for retrieving XCO_2 from GOSAT and OCO-2 measurements, the different impacts of XCO_2 data on land sinks may be related to the spatial coverage and the amount of data in these two XCO_2 datasets. As shown in Fig. 1, in different latitude zones, the spatial coverage and the data amount of GOSAT and OCO-2 have large differences. Statistics show that the amount of data is largest in northern temperate land, followed by southern temperate land and tropical land; it is smallest in northern boreal regions, corresponding to the magnitude of changes in carbon fluxes in these zones. For one specific zone, the different impacts of these two XCO_2 datasets may also be related to the data amount. For example, in northern temperate land, GOSAT has more XCO_2 data than OCO-2. Accordingly, the change in carbon flux caused by GOSAT is larger than that caused by OCO-2. Conversely, in tropical land, OCO-2 has more data than GOSAT, and as shown before it has a more significant impact on the land sink. This relationship could also be found in each TRANSCOM region. Figure 5 gives a relationship between the XCO_2 data amount ratios of GOSAT to OCO-2 and the land sink absolute change ratios caused by GOSAT to OCO-2 for 11 TRANSCOM land regions. Obviously, except for North and South Africa, there is a significant linear correlation ($R = 0.95$) between these two ratios, suggesting that with more XCO_2 data, the carbon flux relative to the prior flux is changed more. In North Africa, we find that OCO-2 has better spatial coverage and more data than GOSAT, as shown in Fig. 1. Although the differences mainly occur in the Sahara where the carbon flux is very weak but near the equatorial region where the carbon flux is large, OCO-2 still has more data than GOSAT. In South Africa, both XCO_2 have good spatial coverage, and the amount of GOSAT data is about 1.5 times that of OCO-2, but the changes in the carbon flux caused by GOSAT are about 10 times that of OCO-2. The large ratio of carbon change is mainly due to the relatively small carbon change from OCO-2 inversion.

In addition to the data amount, mismatches between the simulated CO_2 concentrations using prior fluxes and satellite retrievals could be used to examine the performances of OCO-2 and GOSAT retrievals in different regions. Usually, a large model–data mismatch will impose a strong constraint on the prior flux in inversions. Therefore, we compare the mismatches in OCO-2 and GOSAT inversions. The results are grouped by global land and into the 11 TRANSCOM land regions, as shown in Table 4. The global land mean difference between modeled XCO_2 and the OCO-2 and GOSAT retrievals are 0.22 and 0.79 ppm, respectively, indicating that the GOSAT retrieval would have a stronger constraint on the prior fluxes. In most TRANSCOM regions except North Africa, the mismatches in GOSAT inversion are positive and larger than those of the OCO-2 inversion. In tropical Asia and the South American tropics, the sizable negative mismatches in OCO-2 inversion could account for a weak inverted carbon sink and an inverted carbon source in these

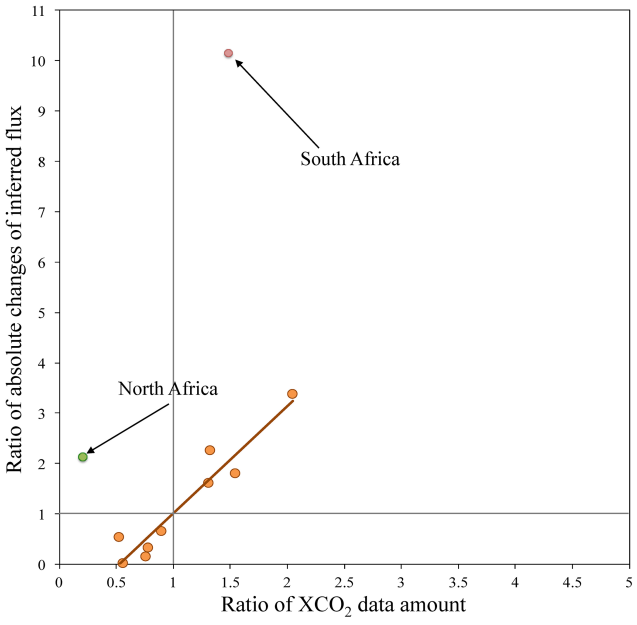

Figure 7. Scatter plot for the ratio of GOSAT to OCO-2 XCO_2 data amount versus the ratio of absolute changes in the land sinks caused by GOSAT to OCO-2 in the 11 TRANSCOM land regions.

two regions, while in North Africa, the negative mismatch in GOSAT inversion may explain why a rather weak sink is inverted for this region. The difference of mismatch between OCO-2 and GOSAT inversions exhibits a rather large spread, ranging from 0.16 to 1.33 pm, indicating that the biases of the two satellite XCO_2 retrievals differ greatly.

Moreover, the uncertainties of OCO-2 and GOSAT retrievals may be another reason for the different performances in these two inversion experiments. We use the TCCON retrieval to evaluate the uncertainties of OCO-2 and GOSAT XCO_2 retrievals. For satellite retrievals falling in the model grid box in which TCCON sites are located, the closest TCCON retrievals in time or within 2 h of satellite overpass time are chosen for comparison. We follow the procedures in Appendix A of Wunch et al. (2011) to create both a prior profile and averaging kernel corrections. Table 5 shows the biases and standard deviations grouped globally and at 10 TCCON sites where both OCO-2 and GOSAT retrievals are available for comparison. The locations of these 10 sites are shown in Fig. 2. At most sites except Garm, OCO-2 retrievals have positive biases, while GOSAT retrievals tend to have negative bias except at the Bial and Garm sites. It also could be found that the spread of GOSAT data biases are small, falling in the range of -0.36 to -0.58 ppm at most sites, while the spread of OCO-2 data biases is relatively large, with biases greater than 0.7 ppm at more than half of the sites and in the range of 0.34 to 0.59 ppm only at three sites. Overall, GOSAT retrievals (-0.46 ppm) have a lower bias than OCO-2 retrievals (0.6 ppm), and the difference between the two retrievals is relatively large. It should be noted that due to the

Table 4. Differences between the inferred and the prior carbon fluxes, the data amount of XCO_2, and the deviations between the XCO_2 modeled with prior flux and satellite-retrieved XCO_2 in different regions.

Region	Flux change ($PgC\,yr^{-1}$)*		XCO_2 data amount		Deviations (ppm)**	
	OCO-2	GOSAT	OCO-2	GOSAT	OCO-2	GOSAT
North American boreal	−0.05	0	1143	639	0.6	1.41
North American temperate	−0.18	−0.41	2390	3163	0.52	0.93
South American tropical	0.46	0.24	800	421	−0.89	0.43
South American temperate	−0.15	−0.5	1711	3500	0.02	0.54
North Africa	0.19	0.39	3208	674	0.12	−0.19
South Africa	−0.03	0.3	2057	3060	0.17	0.33
Eurasian boreal	0.05	−0.02	1714	1339	0.47	1.5
Eurasian temperate	−0.46	−0.3	5323	4782	0.46	0.82
Tropical Asia	0.17	0.03	726	550	−0.43	0.34
Australia	−0.05	−0.1	2011	3110	0.18	0.67
Europe	−0.39	−0.63	1604	2106	0.28	1.35
Global land	−0.44	−0.98	22687	23344	0.22	0.79
Northern boreal land	0.005	−0.02	2857	1978	0.52	1.47
Northern temperate land	−1.03	−1.33	9317	10051	0.45	0.96
Tropical land	0.82	0.66	4734	1645	−0.08	0.13
Southern temperate land	−0.234	−0.3	5779	9670	0.11	0.6

* Differences between posterior and prior flux. ** Deviations between the modeled XCO_2 with prior flux and satellite-retrieved XCO_2.

Table 5. Statistics of the OCO-2 and GOSAT retrieval uncertainties against the TCCON retrievals.

	OCO-2			GOSAT		
	Bias (ppm)	SD (ppm)	No. of obs.	Bias (ppm)	SD (ppm)	No. of obs.
Bial	0.91	1.47	21	0.06	1.35	29
Darw	0.75	0.85	43	−0.41	1.62	44
Garm	−0.10	2.97	14	0.73	2.02	35
Lamo	0.04	1.09	56	−0.91	1.39	82
Laud	0.59	1.38	18	−0.79	1.70	30
Orle	1.49	1.18	24	−0.51	1.38	39
Park	0.50	1.26	29	−0.58	1.52	38
Soda	1.91	1.89	7	−0.54	2.58	9
Tsuk	0.93	1.95	16	−0.47	1.11	38
Woll	0.34	1.07	27	−0.36	1.56	45
All	0.60	1.45	255	−0.42	1.59	389

limited number of collocated satellite retrievals, the real bias difference might be below 1 ppm. As shown in Table 4, the difference of overall mismatches between GOSAT and OCO-2 data is 0.57 ppm. This indicates that although both OCO-2 and GOSAT products were bias-corrected using TCCON retrievals, the uncertainties of OCO-2 and GOSAT retrievals are still very large, especially for the OCO-2 retrieval, resulting in a degraded performance of the OCO-2 retrieval, which also suggests that the bias-correction scheme implemented may need to be improved.

5 Summary and conclusions

In this study, we use both GOSAT and OCO-2 XCO_2 retrievals to constrain terrestrial ecosystem carbon fluxes from 1 October 2014 to 31 December 2015 using the GEOS-Chem 4D-Var data assimilation system. In addition, one inversion using in situ measurements and another inversion as a baseline are also conducted. The posterior carbon fluxes estimated from these four inversions at both global and regional scales during 1 January to 31 December 2015 are shown and discussed. We evaluate the posterior carbon fluxes by comparing the posterior CO_2 mixing ratios against observations from 52 surface flask sites and 13 TCCON sites.

Globally, the terrestrial ecosystem carbon sink (excluding biomass burning emissions) estimated from GOSAT data is stronger than that inferred from OCO-2 data and weaker than that from in situ inversion, but it is closest to the poor-man inversion estimate. Regionally, in most regions, the land sinks inferred from GOSAT data are also stronger than those from OCO-2 data. Compared with the in situ inversion, GOSAT inversions have weaker sinks in boreal and most tropical lands and much stronger ones in temperate lands. Compared with the prior fluxes, the inferred land sinks are largely increased in the temperate regions and decreased in tropical regions. The largest changes in the prior fluxes are in northern temperate regions, followed by tropical and southern temperate regions, and the weakest are in boreal regions. The different impact of XCO_2 on the carbon fluxes in different regions is mainly related to the spatial coverage and the amount of XCO_2 data. Generally, a larger amount of XCO_2 data in a region corresponds to a larger change in the inverted carbon flux in the same region. The different biases of the two XCO_2 retrievals may also give rise to their different inversion performances.

Evaluations of inversions using CO_2 concentrations from flask measurements and TCCON retrievals show that the simulated CO_2 concentrations with GOSAT posterior fluxes are much closer to the observations than those with OCO-2 estimates. Compared with poor-man inversion, both GOSAT and in situ inversions show evident improvement, with similar reductions of both the biases and standard deviations of posterior concentrations, while OCO-2 inversion only displays slight improvement over poor-man inversion. Generally, the posterior biases from GOSAT inversion are significantly reduced in the Northern Hemisphere and are slightly increased in the Southern Hemisphere. This suggests that GOSAT data can effectively improve carbon flux estimates in the Northern Hemisphere.

The GOSAT and OCO-2 XCO_2 retrievals used in this study are bias-corrected products. Nevertheless, there are still apparent biases, and the differences between the data from these two satellites are obvious. More reliable constraints on carbon flux call for the further reduction of satellite retrieval errors. This indicates that we should interpret the carbon flux inferred from current satellite XCO_2 retrievals with great caution in understanding the global carbon cycle. It also should be noted that though the OCO-2 XCO_2 retrievals of version b7.3 used in this study perform worse than GOSAT data and in situ measurements in our inversions, one recent study has shown that the newer version of OCO-2 data has a much better performance in constraining carbon flux (Chevallier et al., 2019). With constantly improved retrieval algorithms and bias-correction schemes, more robust estimates of carbon flux from satellite XCO_2 retrievals could be achieved.

Data availability. The inversion results are available to the community and can be accessed upon request from Fei Jiang (jiangf@nju.edu.cn) at Nanjing University.

Author contributions. FJ and HW designed the research, HW conducted inverse modeling, HW and FJ conducted data analysis and wrote the paper, and JW, WJ and JC participated in the discussion of the results and provided input on the paper for revision before submission.

Competing interests. The authors declare that they have no conflict of interest.

Special issue statement. This article is part of the special issue "The 10th International Carbon Dioxide Conference (ICDC10) and the 19th WMO/IAEA Meeting on Carbon Dioxide, other Greenhouse Gases and Related Measurement Techniques (GGMT-2017) (AMT/ACP/BG/CP/ESD inter-journal SI)". It is a result of the 10th International Carbon Dioxide Conference, Interlaken, Switzerland, 21–25 August 2017.

Acknowledgements. The authors thank all contributing laboratories for providing in situ CO_2 observations through the ObsPack product obspack_co2_1_CARBONTRACKER_CT2016_2017-02-06 and TCCON PIs for making XCO_2 measurements possible and available to the public. CarbonTracker CT2016 products are provided by NOAA ESRL, Boulder, Colorado, USA, from the website at http://carbontracker.noaa.gov (last access: 10 August 2017). The authors are very grateful to Feng Deng at the University of Toronto for providing the module for in situ data inversion and for his valuable suggestions on running the GEOS-Chem adjoint model. The authors would also like to thank Dr. Wouter Peters and one anonymous referee for their constructive comments and suggestions, which greatly improved the paper.

Financial support. This research has been supported by the National Key R&D Program of China (grant no. 2016YFA0600204), and the National Natural Science Foundation of China (grant no. 41571452).

Review statement. This paper was edited by Christoph Gerbig and reviewed by Wouter Peters and one anonymous referee.

References

Andres, R. J., Gregg, J. S., Losey, L., Marland, G., and Boden, T. A.: Monthly, global emissions of carbon dioxide from fossil fuel consumption. Tellus B, 63, 309–327, https://doi.org/10.1111/j.1600-0889.2011.00530.x, 2011.

Baker, D. F., Bösch, H., Doney, S. C., O'Brien, D., and Schimel, D. S.: Carbon source/sink information provided by column CO_2

measurements from the Orbiting Carbon Observatory, Atmos. Chem. Phys., 10, 4145–4165, https://doi.org/10.5194/acp-10-4145-2010, 2010.

Basu, S., Guerlet, S., Butz, A., Houweling, S., Hasekamp, O., Aben, I., Krummel, P., Steele, P., Langenfelds, R., Torn, M., Biraud, S., Stephens, B., Andrews, A., and Worthy, D.: Global CO_2 fluxes estimated from GOSAT retrievals of total column CO_2, Atmos. Chem. Phys., 13, 8695–8717, https://doi.org/10.5194/acp-13-8695-2013, 2013.

Blumenstock, T., Hase, F., Schneider, M., García, O. E., and Sepúlveda, E.: TCCON data from Izana, Tenerife, Spain, Release GGG2014R1, TCCON data archive, hosted by CaltechDATA, California Institute of Technology, Pasadena, CA, USA, https://doi.org/10.14291/tccon.ggg2014.izana01.R1, 2017.

Byrd, R. H., Nocedal, J., and Schnabel, R. B.: Representations of Quasi-Newton Matrices and their use in Limited Memory Methods, Math Program. 63, 129–156, https://doi.org/10.1007/BF01582063, 1994.

CarbonTracker Team: Simulated observations of atmospheric carbon dioxide from CarbonTracker release CT2016 (obspack_co2_1_ CARBONTRACKER_CT2016_2017-02-06); NOAA Earth System Research Laboratory, Global Monitoring Division, https://doi.org/10.15138/G3G599, 2017.

Chatterjee, A., Gierach, M. M., Sutton, A. J., Feely, R. A., Crisp, D., Eldering, A., Gunson, M. R., O'Dell, C. W., Stephens, B. B., and Schimel, D. S.: Influence of El Niño on atmospheric CO_2 over the tropical Pacific Ocean: Findings from NASA's OCO-2 mission, Science, 358, eaam5776, https://doi.org/10.1126/science.aam5776, 2017.

Chevallier, F., Breon, F.-M., and Rayner, P. J.: Contribution of the Orbiting Carbon Observatory to the estimation of CO_2 sources and sinks: Theoretical study in a variational data assimilation framework, J. Geophys. Res.-Atmos., 112, d09307, https://doi.org/10.1029/2006JD007375, 2007.

Chevallier, F., Engelen, R. J., Carouge, C., Conway, T. J., Peylin, P.,Pickett-Heaps, C., Ramonet, M., Rayner, P. J., and Xueref-Remy, I.: AIRS-based versus flask-based estimation of carbon surface fluxes, J. Geophys. Res., 114, D20303, https://doi.org/10.1029/2009JD012311, 2009.

Chevallier, F., Ciais, P., Conway, T. J., Aalto, T., Anderson, B. E., Bousquet, P., Brunke, E. G., Ciattaglia, L., Esaki, Y., Fröhlich, M., Gomez, A., Gomez-Pelaez, A. J., Haszpra, L., Krummel, P. B., Langenfelds, R. L., Leuenberger, M., Machida, T., Maignan, F., Matsueda, H., Morguí, J. A., Mukai, H., Nakazawa, T., Peylin, P., Ramonet, M., Rivier, L., Sawa, Y., Schmidt, M., Steele, L. P., Vay, S. A., Vermeulen, A. T., Wofsy, S., and Worthy, D.: CO_2 surface fluxes at grid point scale estimated from a global 21 year reanalysis of atmospheric measurements, J. Geophys. Res., 115, D21307, https://doi.org/10.1029/2010JD013887, 2010.

Chevallier, F., Palmer, P. I., Feng, L., Boesch, H., O'Dell, C. W., and Bousquet, P.: Toward robust and consistent regional CO_2 flux estimates from in situ and spaceborne measurements of atmospheric CO_2, Geophys. Res. Lett., 41, 1065–1070, https://doi.org/10.1002/2013GL058772, 2014.

Chevallier, F., Remaud, M., O'Dell, C. W., Baker, D., Peylin, P., and Cozic, A.: Objective evaluation of surface- and satellite-driven CO_2 atmospheric inversions, Atmos. Chem. Phys. Discuss., https://doi.org/10.5194/acp-2019-213, in review, 2019.

Crisp, D., Pollock, H. R., Rosenberg, R., Chapsky, L., Lee, R. A. M., Oyafuso, F. A., Frankenberg, C., O'Dell, C. W., Bruegge, C. J., Doran, G. B., Eldering, A., Fisher, B. M., Fu, D., Gunson, M. R., Mandrake, L., Osterman, G. B., Schwandner, F. M., Sun, K., Taylor, T. E., Wennberg, P. O., and Wunch, D.: The on-orbit performance of the Orbiting Carbon Observatory-2 (OCO-2) instrument and its radiometrically calibrated products, Atmos. Meas. Tech., 10, 59–81, https://doi.org/10.5194/amt-10-59-2017, 2017.

Deng, F. and Chen, J. M.: Recent global CO_2 flux inferred from atmospheric CO_2 observations and its regional analyses, Biogeosciences, 8, 3263–3281, https://doi.org/10.5194/bg-8-3263-2011, 2011.

Deng, F., Jones, D. B. A., Henze, D. K., Bousserez, N., Bowman, K. W., Fisher, J. B., Nassar, R., O'Dell, C., Wunch, D., Wennberg, P. O., Kort, E. A., Wofsy, S. C., Blumenstock, T., Deutscher, N. M., Griffith, D. W. T., Hase, F., Heikkinen, P., Sherlock, V., Strong, K., Sussmann, R., and Warneke, T.: Inferring regional sources and sinks of atmospheric CO_2 from GOSAT XCO_2 data, Atmos. Chem. Phys., 14, 3703–3727, https://doi.org/10.5194/acp-14-3703-2014, 2014.

Deng, F., Jones, D. B. A., O'Dell, C. W., Nassar, R., and Parazoo, N. C.: Combining GOSAT XCO_2 observations over land and ocean to improve regional CO_2 flux estimates, J. Geophys. Res.-Atmos., 121, 1896–1913, https://doi.org/10.1002/2015JD024157, 2016.

Deutscher, N., Notholt, J., Messerschmidt, J., Weinzierl, C., Warneke, T., Petri, C., Grupe, P., and Katrynski, K.: TCCON data from Bialystok, Poland, Release GGG2014R1, TCCON data archive, hosted by CaltechDATA, California Institute of Technology, Pasadena, CA, USA, https://doi.org/10.14291/tccon.ggg2014.bialystok01.R1/1183984, 2017.

Eldering, A., Boland, S., Solish, B., Crisp, D., Kahn, P., and Gunson, M.: High precision atmospheric CO_2 measurements from space: The design and implementation of OCO-2, in: 2012 IEEE Aerospace Conference, 1–10, https://doi.org/10.1109/AERO.2012.6187176, 2012.

Eldering, A., O'Dell, C. W., Wennberg, P. O., Crisp, D., Gunson, M. R., Viatte, C., Avis, C., Braverman, A., Castano, R., Chang, A., Chapsky, L., Cheng, C., Connor, B., Dang, L., Doran, G., Fisher, B., Frankenberg, C., Fu, D., Granat, R., Hobbs, J., Lee, R. A. M., Mandrake, L., McDuffie, J., Miller, C. E., Myers, V., Natraj, V., O'Brien, D., Osterman, G. B., Oyafuso, F., Payne, V. H., Pollock, H. R., Polonsky, I., Roehl, C. M., Rosenberg, R., Schwandner, F., Smyth, M., Tang, V., Taylor, T. E., To, C., Wunch, D., and Yoshimizu, J.: The Orbiting Carbon Observatory-2: first 18 months of science data products, Atmos. Meas. Tech., 10, 549–563, https://doi.org/10.5194/amt-10-549-2017, 2017a.

Eldering, A., Wennberg, P. O., Crisp, D., Schimel, D. S., Gunson, M. R., Chatterjee, A., Liu, J., Schwandner, F. M., Sun, Y., O'Dell, C. W., Frankenberg, C., Taylor, T., Fisher, B., Osterman, G. B., Wunch, D., Hakkarainen, J., Tamminen, J., and Weir, B.: The Orbiting Carbon Observatory-2 early science investigations of regional carbon dioxide fluxes, Science, 358, eaam5745, https://doi.org/10.1126/science.aam5745, 2017b.

Feng, L., Palmer, P. I., Parker, R. J., Deutscher, N. M., Feist, D. G., Kivi, R., Morino, I., and Sussmann, R.: Estimates of European uptake of CO_2 inferred from GOSAT XCO_2 retrievals: sensitivity to measurement bias inside and outside Europe, At-

mos. Chem. Phys., 16, 1289–1302, https://doi.org/10.5194/acp-16-1289-2016, 2016.

Giglio, L., Randerson, J. T., and van der Werf, G. R.: Analysis of daily, monthly, and annual burned area using the fourth-generation global fire emissions database (GFED4) J. Geophys. Res.-Biogeosci., 118, 317–328, https://doi.org/10.1002/jgrg.20042, 2013.

Griffith, D. W. T., Deutscher, N., Velazco, V. A., Wennberg, P. O., Yavin, Y., Keppel Aleks, G., Washenfelder, R., Toon, G. C., Blavier, J.-F., Murphy, C., Jones, N., Kettlewell, G., Connor, B., Macatangay, R., Roehl, C., Ryczek, M., Glowacki, J., Culgan, T., and Bryant, G.: TCCON data from Darwin, Australia, Release GGG2014R0. TCCON data archive, hosted by CaltechDATA, California Institute of Technology, Pasadena, CA, USA, https://doi.org/10.14291/tccon.ggg2014.darwin01.R0/1149290, 2017a.

Griffith, D. W. T., Velazco, V. A., Deutscher, N., Murphy, C., Jones, N., Wilson, S., Macatangay, R., Kettlewell, G., Buchholz, R. R., and Riggenbach, M.: TCCON data from Wollongong, Australia, Release GGG2014R0. TCCON data archive, hosted by CaltechDATA, California Institute of Technology, Pasadena, CA, USA, https://doi.org/10.14291/tccon.ggg2014.wollongong01.R0/1149291, 2017b.

Gurney, K. R., Law, R. M., Denning, A. S., Rayner, P. J., Baker, D., Bousquet, P., Bruhwiler, L., Chen, Y.-H., Ciais, P., Fan, S., Fung, I. Y., Gloor, M., Heimann, M., Higuchi, K., John, J., Maki, T., Maksyutov, S., Masarie, K., Peylin, P., Prather, M., Pak, B. C., Randerson, J., Sarmiento, J., Taguchi, S., Takahashi, T., and Yuen, C.-W.: Towards robust regional estimates of CO_2 sources and sinks using atmospheric transport models, Nature, 415, 626–630, 2002.

Henze, D. K., Hakami, A., and Seinfeld, J. H.: Development of the adjoint of GEOS-Chem, Atmos. Chem. Phys., 7, 2413–2433, https://doi.org/10.5194/acp-7-2413-2007, 2007.

Heymann, J., Reuter, M., Buchwitz, M., Schneising, O., Bovensmann, H., Burrows, J. P., Massart, S., Kaiser, J. W., and Crisp, D.: CO_2 emission of Indonesian fires in 2015 estimated from satellite-derived atmospheric CO_2 concentrations, Geophys. Res. Lett., 44, 1537–1544, https://doi.org/10.1002/2016GL072042, 2017.

Houweling, S., Breon, F.-M., Aben, I., Rödenbeck, C., Gloor, M., Heimann, M., and Ciais, P.: Inverse modeling of CO_2 sources and sinks using satellite data: a synthetic inter-comparison of measurement techniques and their performance as a function of space and time, Atmos. Chem. Phys., 4, 523–538, https://doi.org/10.5194/acp-4-523-2004, 2004.

Houweling, S., Baker, D., Basu, S., Boesch, H., Butz, A., Chevallier, F., Deng, F., Dlugokencky, E. J., Feng, L., Ganshin, A., Hasekamp, O., Jones, D., Maksyutov, S., Marshall, J., Oda, T., O'Dell, C. W., Oshchepkov, S., Palmer, P. I., Peylin, P., Poussi, Z., Reum, F., Takagi, H., Yoshida, Y., and Zhuravlev, R.: An intercomparison of inverse models for estimating sources and sinks of CO_2 using GOSAT measurements, J. Geophys. Res.-Atmos., 120, 5253–5266, https://doi.org/10.1002/2014JD022962, 2015.

Hungershoefer, K., Breon, F.-M., Peylin, P., Chevallier, F., Rayner, P., Klonecki, A., Houweling, S., and Marshall, J.: Evaluation of various observing systems for the global monitoring of CO_2 surface fluxes, Atmos. Chem. Phys., 10, 10503–10520, https://doi.org/10.5194/acp-10-10503-2010, 2010.

Jiang, Z., Jones, D. B. A., Kopacz, M., Liu, J., Henze, D. K., and Heald, C.: Quantifying the impact of model errors on top-down estimates of carbon monoxide emissions using satellite observations, J. Geophys. Res., 116, D15306, https://doi.org/10.1029/2010JD015282, 2011.

Kadygrov, N., Maksyutov, S., Eguchi, N., Aoki, T., Nakazawa, T., Yokota, T., and Inoue, G.: Role of simulated GOSAT total column CO2 observations in surface CO_2 flux uncertainty reduction, J. Geophys. Res., 114, D21208, https://doi.org/10.1029/2008JD011597, 2009.

Kivi, R., Heikkinen, P., and Kyro, E.: TCCON data from Sodankyla, Finland, Release GGG2014R0. TCCON data archive, hosted by CaltechDATA, California Institute of Technology, Pasadena, CA, USA, https://doi.org/10.14291/tccon.ggg2014.sodankyla01.R0/1149280, 2017.

Kopacz, M., Jacob, D. J., Henze, D. K., Heald, C. L., Streets, D. G., and Zhang, Q.: A comparison of analytical and adjoint Bayesian inversion methods for constraining Asian sources of CO using satellite (MOPITT) measurements of CO columns, J. Geophys. Res., 114, D04305, https://doi.org/10.1029/2007JD009264, 2009.

Kopacz, M., Jacob, D. J., Fisher, J. A., Logan, J. A., Zhang, L., Megretskaia, I. A., Yantosca, R. M., Singh, K., Henze, D. K., Burrows, J. P., Buchwitz, M., Khlystova, I., McMillan, W. W., Gille, J. C., Edwards, D. P., Eldering, A., Thouret, V., and Nedelec, P.: Global estimates of CO sources with high resolution by adjoint inversion of multiple satellite datasets (MOPITT, AIRS, SCIAMACHY, TES), Atmos. Chem. Phys., 10, 855–876, https://doi.org/10.5194/acp-10-855-2010, 2010.

Kuze, A., Suto, H., Nakajima, M., and Hamazaki, T.: Thermal and near infrared sensor for carbon observation Fourier-transform spectrometer on the Greenhouse Gases Observing Satellite for greenhouse gases monitoring, Appl. Opt., 48, 6716, https://doi.org/10.1364/AO.48.006716, 2009.

Liu, J., Bowman, K. W., Lee, M., Henze, D. K., Bousserez, N., Brix, H., Collatz, G. J., Menemenlis, D., Ott, L., Pawson, S., Jones, D., and Nassar, R.: Carbon monitoring system flux estimation and attribution: impact of ACOS-GOSAT XCO_2 sampling on the inference of terrestrial biospheric sources and sinks, Tellus B, 66, 22486, https://doi.org/10.3402/tellusb.v66.22486, 2014.

Liu, J., Bowman, K. W., Schimel, D. S., Parazoo, N. C., Jiang, Z., Lee, M., Bloom, A. A., Wunch, D., Frankenberg, C., Sun, Y., O'Dell, C. W., Gurney, K. R., Menemenlis, D., Gierach, M., Crisp, D., and Eldering, A.: Contrasting carbon cycle responses of the tropical continents to the 2015–2016 El Niño, Science, 358, eaam5690, https://doi.org/10.1126/science.aam5690, 2017.

Maksyutov, S., Takagi, H., Valsala, V. K., Saito, M., Oda, T., Saeki, T., Belikov, D. A., Saito, R., Ito, A., Yoshida, Y., Morino, I., Uchino, O., Andres, R. J., and Yokota, T.: Regional CO_2 flux estimates for 2009–2010 based on GOSAT and ground-based CO_2 observations, Atmos. Chem. Phys., 13, 9351–9373, https://doi.org/10.5194/acp-13-9351-2013, 2013.

Messerschmidt, J., Geibel, M. C., Blumenstock, T., Chen, H., Deutscher, N. M., Engel, A., Feist, D. G., Gerbig, C., Gisi, M., Hase, F., Katrynski, K., Kolle, O., Lavrič, J. V., Notholt, J., Palm, M., Ramonet, M., Rettinger, M., Schmidt, M., Sussmann, R., Toon, G. C., Truong, F., Warneke, T., Wennberg, P. O., Wunch, D., and Xueref-Remy, I.: Calibration of TCCON

column-averaged CO_2: the first aircraft campaign over European TCCON sites, Atmos. Chem. Phys., 11, 10765–10777, https://doi.org/10.5194/acp-11-10765-2011, 2011.

Miller, C. E., Crisp, D., DeCola, P. L., Olsen, S. C., Randerson, J. T., Michalak, A. M., Alkhaled, A., Rayner, P., Jacob, D. J., Suntharalingam, P., Jones, D. B. A., Denning, A. S., Nicholls, M. E., Doney, S. C., Pawson, S., Boesch, H., Connor, B. J., Fung, I. Y., O'Brien, D., Salawitch, R. J., Sander, S. P., Sen, B., Tans, P., Toon, G. C., Wennberg, P. O., Wofsy, S. C., Yung, Y. L., and Law, R. M.: Precision requirements for space-based XCO_2 data, J. Geophys. Res., 112, D10314, https://doi.org/10.1029/2006JD007659, 2007.

Miller, S. M., Michalak, A. M., Yadav, V., and Tadić, J. M.: Characterizing biospheric carbon balance using CO_2 observations from the OCO-2 satellite, Atmos. Chem. Phys., 18, 6785–6799, https://doi.org/10.5194/acp-18-6785-2018, 2018.

Morino, I., Matsuzaki, T., and Shishime, A.: TCCON data from Tsukuba, Ibaraki, Japan, 125HR, Release GGG2014R2. TCCON data archive, hosted by CaltechDATA, California Institute of Technology, Pasadena, CA, USA, https://doi.org/10.14291/tccon.ggg2014.tsukuba02.R2, 2017.

Nassar, R., Jones, D. B. A., Suntharalingam, P., Chen, J. M., Andres, R. J., Wecht, K. J., Yantosca, R. M., Kulawik, S. S., Bowman, K. W., Worden, J. R., Machida, T., and Matsueda, H.: Modeling global atmospheric CO_2 with improved emission inventories and CO_2 production from the oxidation of other carbon species, Geosci. Model Dev., 3, 689–716, https://doi.org/10.5194/gmd-3-689-2010, 2010.

Nassar, R., Hill, T. G., McLinden, C. A., Wunch, D., Jones, D. B. A., and Crisp, D.: Quantifying CO_2 emissions From Individual Power Plants from Space, Geophys. Res. Lett., 44, 10045–10053, https://doi.org/10.1002/2017GL074702, 2017.

Notholt, J., Petri, C., Warneke, T., Deutscher, N., Buschmann, M., Weinzierl, C., Macatangay, R., and Grupe, P.: TCCON data from Bremen, Germany, Release GGG2014R0. TCCON data archive, hosted by CaltechDATA, California Institute of Technology, Pasadena, CA, USA, https://doi.org/10.14291/tccon.ggg2014.bremen01.R0/1149275, 2017a.

Notholt, J., Schrems, O., Warneke, T., Deutscher, N., Weinzierl, C., Palm, M., Buschmann, M., and AWI-PEV Station Engineers: TCCON data from Ny Alesund, Spitzbergen, Norway, Release GGG2014R0. TCCON data archive, hosted by CaltechDATA, California Institute of Technology, Pasadena, CA, USA, https://doi.org/10.14291/tccon.ggg2014.nyalesund01.R0/1149278, 2017b.

ObsPack: Cooperative Global Atmospheric Data Integration Project, Multi-laboratory compilation of atmospheric carbon dioxide data for the period 1957–2015, obspack_co2_1_GLOBALVIEWplus_v2.1_2016-09-02, NOAA Earth System Research Laboratory, Global Monitoring Division, https://doi.org/10.15138/G3059Z, 2016.

O'Dell, C. W., Connor, B., Bösch, H., O'Brien, D., Frankenberg, C., Castano, R., Christi, M., Eldering, D., Fisher, B., Gunson, M., McDuffie, J., Miller, C. E., Natraj, V., Oyafuso, F., Polonsky, I., Smyth, M., Taylor, T., Toon, G. C., Wennberg, P. O., and Wunch, D.: The ACOS CO_2 retrieval algorithm – Part 1: Description and validation against synthetic observations, Atmos. Meas. Tech., 5, 99–121, https://doi.org/10.5194/amt-5-99-2012, 2012.

Oda, T. and Maksyutov, S.: A very high-resolution (1 km × 1 km) global fossil fuel CO_2 emission inventory derived using a point source database and satellite observations of nighttime lights, Atmos. Chem. Phys., 11, 543–556, https://doi.org/10.5194/acp-11-543-2011, 2011.

Park, B. C. and Prather, M. J.: CO_2 source inversions using satellite observations of the upper troposphere, Geophys. Res. Lett., 28, 4571–4574, https://doi.org/10.1029/2001GL013604, 2001.

Parrington, M., Palmer, P. I., Henze, D. K., Tarasick, D. W., Hyer, E. J., Owen, R. C., Helmig, D., Clerbaux, C., Bowman, K. W., Deeter, M. N., Barratt, E. M., Coheur, P.-F., Hurtmans, D., Jiang, Z., George, M., and Worden, J. R.: The influence of boreal biomass burning emissions on the distribution of tropospheric ozone over North America and the North Atlantic during 2010, Atmos. Chem. Phys., 12, 2077–2098, https://doi.org/10.5194/acp-12-2077-2012, 2012.

Patra, P. K., Crisp, D., Kaiser, J. W., Wunch, D., Saeki, T., Ichii, K., Sekiya, T., Wennberg, P. O., Feist, D. G., Pollard, D. F., Griffith, D. W. T., Velazco, V. A., De Maziere, M., Sha, M. K., Roehl, C., Chatterjee, A., and Ishijima, K.: The Orbiting Carbon Observatory (OCO-2) tracks 2–3 peta-gram increase in carbon release to the atmosphere during the 2014–2016 El Niño, Sci. Rep.-UK, 7, 13567, https://doi.org/10.1038/s41598-017-13459-0, 2017.

Peters, W., Jacobson, A. R., Sweeney, C., Andrews, A. E., Conway, T. J., Masarie, K., Miller, J. B., Bruhwiler, L. M. P., P'etron, G., Hirsch, A. I.,Worthy, D. E. J.,Werf, G. R. V. D., Randerson, J. T., Wennberg, P. O., Krol, M. C., and Tans, P. P.: An atmospheric perspective on North American carbon dioxide exchange: CarbonTracker, P. Natl. Acad. Sci. USA, 104, 18925–18930, 2007..

Peylin, P., Law, R. M., Gurney, K. R., Chevallier, F., Jacobson, A. R., Maki, T., Niwa, Y., Patra, P. K., Peters, W., Rayner, P. J., Rödenbeck, C., van der Laan-Luijkx, I. T., and Zhang, X.: Global atmospheric carbon budget: results from an ensemble of atmospheric CO_2 inversions, Biogeosciences, 10, 6699–6720, https://doi.org/10.5194/bg-10-6699-2013, 2013.

Potter, C. S., Randerson, J. T., Field, C. B., Matson, P. A., Vitousek, P. M., Mooney, H. A., and Klooster, S. A.: Terrestrial ecosystem production: A process model based on global satellite and surface data, Global Biogeochem. Cy., 7, 811–841, https://doi.org/10.1029/93GB02725, 1993.

Rayner, P. J. and O'Brien, D. M.: The utility of remotely sensed CO_2 concentration data in surface source inversions, Geophys. Res. Lett., 28, 175–178, https://doi.org/10.1029/2000GL011912, 2001.

Reuter, M., Buchwitz, M., Hilker, M., Heymann, J., Schneising, O., Pillai, D., Bovensmann, H., Burrows, J. P., Bösch, H., Parker, R., Butz, A., Hasekamp, O., O'Dell, C. W., Yoshida, Y., Gerbig, C., Nehrkorn, T., Deutscher, N. M., Warneke, T., Notholt, J., Hase, F., Kivi, R., Sussmann, R., Machida, T., Matsueda, H., and Sawa, Y.: Satellite-inferred European carbon sink larger than expected, Atmos. Chem. Phys., 14, 13739–13753, https://doi.org/10.5194/acp-14-13739-2014, 2014.

Reuter, M., Buchwitz, M., Hilker, M., Heymann, J., Bovensmann, H., Burrows, J. P., Houweling, S., Liu, Y. Y., Nassar, R., Chevallier, F., Ciais, P., Marshall, J., and Reichstein, M.: How Much CO_2 Is Taken Up by the European Terrestrial Biosphere?, B. Am. Meteorol. Soc., 98, 665–671, https://doi.org/10.1175/BAMS-D-15-00310.1, 2017.

Rienecker, M. M., Suarez, M. J., Todling, R., Bacmeister, J., Takacs, L., Liu, H.-C., Gu, W., Sienkiewicz, M., Koster, R. D., Gelaro, R., Stajner, I., and Nielsen, E.: The GEOS-5 Data Assimilation System-Documentation of versions 5.0.1 and 5.1.0, and 5.2.0 NASA Tech. Rep. Series on Global Modeling and Data Assimilation, NASA/TM-2008-104606, Vol. 27, 92 pp., 2008.

Rodgers, C. D.: Inverse Methods for Atmospheric Sounding: Theory and Practice, World Scientific Publishing Co Inc, Singapore, chapter 2, 2000.

Saeki, T., Maksyutov, S., Saito, M., Valsala, V., Oda, T., An- dres, R. J., Belikov, D., Tans, P., Dlugokencky, E., Yoshida, Y., Morino, I., Uchino, O., and Yokota, T.: Inverse modeling of CO_2 fluxes using GOSAT data and multi-year ground-based obser- vations, SOLA, 9, 45–50, https://doi.org/10.2151/sola.2013-011, 2013.

Sherlock, V., Connor, B., Robinson, J., Shiona, H., Smale, D., and Pollard, D.: TCCON data from Lauder, New Zealand, 125HR, Release GGG2014R0, TCCON data archive, hosted by CaltechDATA, California Institute of Technology, Pasadena, CA, USA, https://doi.org/10.14291/tccon.ggg2014.lauder02.R0/1149298, 2017.

Singh, K., Jardak, M., Sandu, A., Bowman, K., Lee, M., and Jones, D.: Construction of non-diagonal background error covariance matrices for global chemical data assimilation, Geosci. Model Dev., 4, 299–316, https://doi.org/10.5194/gmd-4-299-2011, 2011.

Suntharalingam, P., Jacob, D. J., Palmer, P. I., Logan, J. A., Yantosca, R. M., Xiao, Y., Evans, M. J., Streets, D. G., Vay, S. L., and Sachse, G. W.: Improved quantification of Chinese carbon fluxes using CO_2/CO correlations in Asian outflow, J. Geophys. Res., 109, D18S18, https://doi.org/10.1029/2003JD004362, 2004.

Sussmann, R. and Rettinger, M.: TCCON data from Garmisch, Germany, Release GGG2014R2. TCCON data archive, hosted by CaltechDATA, California Institute of Technology, Pasadena, CA, USA, https://doi.org/10.14291/tccon.ggg2014.garmisch01.R2, 2017.

Tarantola, A.: Inverse Problem Theory and Methods for Model Parameter Estimation, Soc. Industr. Appl. Math., Philadelphia, PA, USA, 2004.

van der Werf, G. R., Randerson, J. T., Giglio, L., Collatz, G. J., Mu, M., Kasibhatla, P. S., Morton, D. C., DeFries, R. S., Jin, Y., and van Leeuwen, T. T.: Global fire emissions and the contribution of deforestation, savanna, forest, agricultural, and peat fires (1997–2009), Atmos. Chem. Phys., 10, 11707–11735, https://doi.org/10.5194/acp-10-11707-2010, 2010.

Wang, X., Guo, Z., Huang, Y. P., Fan, H. J., and Li, W. B.: A cloud detection scheme for the Chinese carbon dioxide observation satellite (TANSAT). Adv. Atmos. Sci., 34, 16–25, https://doi.org/10.1007/s00376-016-6033-y, 2017.

Warneke, T., Messerschmidt, J., Notholt, J., Weinzierl, C., Deutscher, N., Petri, C., Grupe, P., Vuillemin, C., Truong, F., Schmidt, M., Ramonet, M., and Parmentier, E.: TCCON data from Orleans, France, Release GGG2014R0. TCCON data archive, hosted by CaltechDATA, California Institute of Technology, Pasadena, CA, USA, https://doi.org/10.14291/tccon.ggg2014.orleans01.R0/1149276, 2017.

Wecht, K. J., Jacob, D. J., Wofsy, S. C., Kort, E. A., Worden, J. R., Kulawik, S. S., Henze, D. K., Kopacz, M., and Payne, V. H.: Validation of TES methane with HIPPO aircraft observations: implications for inverse modeling of methane sources, Atmos. Chem. Phys., 12, 1823–1832, https://doi.org/10.5194/acp-12-1823-2012, 2012.

Wennberg, P. O., Roehl, C., Wunch, D., Toon, G. C., Blavier, J.-F., Washenfelder, R., Keppel-Aleks, G., Allen, N., and Ayers, J.: TCCON data from Park Falls, Wisconsin, USA, Release GGG2014R1, TCCON data archive, hosted by CaltechDATA, California Institute of Technology, Pasadena, CA, USA, https://doi.org/10.14291/tccon.ggg2014.parkfalls01.R1, 2017.

Wennberg, P. O., Wunch, D., Roehl, C., Blavier, J.-F., Toon, G. C., Allen, N., Dowell, P., Teske, K., Martin, C., and Martin, J.: TCCON data from Lamont, Oklahoma, USA, Release GGG2014R1, TCCON data archive, hosted by CaltechDATA, California Institute of Technology, Pasadena, CA, USA, https://doi.org/10.14291/tccon.ggg2014.lamont01.R1/1255070, 2017.

Wunch, D., Toon, G. C., Wennberg, P. O., Wofsy, S. C., Stephens, B. B., Fischer, M. L., Uchino, O., Abshire, J. B., Bernath, P., Biraud, S. C., Blavier, J.-F. L., Boone, C., Bowman, K. P., Browell, E. V., Campos, T., Connor, B. J., Daube, B. C., Deutscher, N. M., Diao, M., Elkins, J. W., Gerbig, C., Gottlieb, E., Griffith, D. W. T., Hurst, D. F., Jiménez, R., Keppel-Aleks, G., Kort, E. A., Macatangay, R., Machida, T., Matsueda, H., Moore, F., Morino, I., Park, S., Robinson, J., Roehl, C. M., Sawa, Y., Sherlock, V., Sweeney, C., Tanaka, T., and Zondlo, M. A.: Calibration of the Total Carbon Column Observing Network using aircraft profile data, Atmos. Meas. Tech., 3, 1351–1362, https://doi.org/10.5194/amt-3-1351-2010, 2010.

Wunch, D., Wennberg, P. O., Toon, G. C., Connor, B. J., Fisher, B., Osterman, G. B., Frankenberg, C., Mandrake, L., O'Dell, C., Ahonen, P., Biraud, S. C., Castano, R., Cressie, N., Crisp, D., Deutscher, N. M., Eldering, A., Fisher, M. L., Griffith, D. W. T., Gunson, M., Heikkinen, P., Keppel-Aleks, G., Kyrö, E., Lindenmaier, R., Macatangay, R., Mendonca, J., Messerschmidt, J., Miller, C. E., Morino, I., Notholt, J., Oyafuso, F. A., Rettinger, M., Robinson, J., Roehl, C. M., Salawitch, R. J., Sherlock, V., Strong, K., Sussmann, R., Tanaka, T., Thompson, D. R., Uchino, O., Warneke, T., and Wofsy, S. C.: A method for evaluating bias in global measurements of CO_2 total columns from space, Atmos. Chem. Phys., 11, 12317–12337, https://doi.org/10.5194/acp-11-12317-2011, 2011.

Wunch, D., Wennberg, P. O., Osterman, G., Fisher, B., Naylor, B., Roehl, C. M., O'Dell, C., Mandrake, L., Viatte, C., Kiel, M., Griffith, D. W. T., Deutscher, N. M., Velazco, V. A., Notholt, J., Warneke, T., Petri, C., De Maziere, M., Sha, M. K., Sussmann, R., Rettinger, M., Pollard, D., Robinson, J., Morino, I., Uchino, O., Hase, F., Blumenstock, T., Feist, D. G., Arnold, S. G., Strong, K., Mendonca, J., Kivi, R., Heikkinen, P., Iraci, L., Podolske, J., Hillyard, P. W., Kawakami, S., Dubey, M. K., Parker, H. A., Sepulveda, E., García, O. E., Te, Y., Jeseck, P., Gunson, M. R., Crisp, D., and Eldering, A.: Comparisons of the Orbiting Carbon Observatory-2 (OCO-2) XCO_2 measurements with TCCON, Atmos. Meas. Tech., 10, 2209–2238, https://doi.org/10.5194/amt-10-2209-2017, 2017.

Yang, D. X., Liu, Y., Cai, Z. N., Chen, X., Yao, L., and Lu, D. R.: First global carbon dioxide maps produced from TanSat measurements, Adv. Atmos. Sci., 35, 621–623, https://doi.org/10.1007/s00376-018-7312-6, 2018.

Zhu, C., Byrd, R. H., Lu, P., and Nocedal, J.: L-BFGS-B: algorithm 778: L-BFGS-B, FORTRAN routines for large scale bound constrained optimization, ACM Trans. Math. Softw., 23, 550–560, https://doi.org/10.1145/279232.279236, 1997.